J. Fluid Mech. (2007), *vol.* 580, *pp.* 451–466.
doi:10.1017/S0022112007005721 Printed in the United Kingdom

Deformation of a droplet adhering to a solid surface in shear flow: onset of interfacial sliding

P. DIMITRAKOPOULOS

Department of Chemical and Biomolecular Engineering, University of Maryland, College Park, MD 20742, USA

(Received 22 July 2006 and in revised form 31 December 2006)

In this paper we consider the dynamics of droplets attached to rough or chemically inhomogeneous solid substrates with a circular contact line as they are deformed in subcritical and supercritical simple shear flows. Our main interest is concentrated on identifying the portions of the contact line where the contact angle hysteresis condition is first violated, i.e. the portions of the contact line which slide first. To address this physical problem, we employ our fully implicit time integration algorithm for interfacial dynamics in Stokes flow. Our study reveals that droplets with small and moderate initial angles show an early period where both upstream and downstream sliding are equally favourable as well as a late downstream-favoured period. By contrast, droplets with large initial angles, after a rather small early equally favourable period, show a large period where downstream sliding is more favourable than the upstream sliding. Owing to the surface tension force, droplets with intermediate initial angles are shown to be more stable. Droplets with different viscosity ratio show similar behaviour with respect to the onset of interfacial sliding; however, the viscosity ratio strongly affects the rate of the interfacial deformation and the equilibrium conditions. An asymptotic behaviour for very small or large viscosity ratios is shown to exist.

1. Introduction

The deformation, sliding and dislodging of fluid droplets adherent to solid substrates constitute a fundamental problem of fluid dynamics with applications in numerous areas including distillation, spray coating, packed towers and a variety of multiphase flow operations in the chemical process industry. Our interest in the problem focuses on viscous flows at low Reynolds number. This regime has relevance in coating operations, enhanced oil recovery, microfluidics and biological systems. In the coating industry, the presence of small liquid droplets or gas bubbles on solid surfaces is a major concern in the design of process equipment, because even a small flow disturbance is sufficient to destroy the uniformity required in precision film coating (Dimitrakopoulos & Higdon 1997). In the petroleum industry, enhanced oil recovery techniques are strongly dependent on the interaction of oil and water in immiscible two-phase mixtures, and the success of such operations depends on the displacement of small oil droplets attached to solid surfaces (Bear 1972). In microfluidics, drop sliding on solid channels is commonly used to produce controlled size droplets and for droplet mixing (e.g. see Cristini & Tan 2004; Stone, Stroock & Ajdari 2004; Tan *et al.* 2004). This problem also provides useful insight into cell spreading (e.g. Greenspan 1978; Hynes 1992; Hodges & Jensen 2002).

The deformation and sliding of fluid droplets attached to rough and chemically inhomogeneous solid surfaces involve several stages because the static contact angle

exhibits a hysteresis effect, i.e. the contact line remains stationary for any angle in the range

$$\theta_R \leqslant \theta \leqslant \theta_A. \tag{1}$$

The limits θ_A and θ_R are called the advancing and receding angles, respectively. (More details concerning the phenomenon of contact angle hysteresis may be found in Dimitrakopoulos & Higdon 1997, 1998).

On such surfaces, under no external forcing conditions, a fluid drop may assume the stable axisymmetric shape of a spherical cap with a constant contact angle θ_0 (with $\theta_R \leqslant \theta_0 \leqslant \theta_A$) around a circular contact line. After the initiation of a shearing flow, the droplet deforms and may break into smaller segments in strong enough flow rates. At the same time, the contact angles change: in the upstream portion of the contact line the contact angles decrease whereas the opposite happens in the downstream portion of the contact line. As long as (1) is satisfied everywhere along the contact line, the shape of the contact line remains unchanged. On the other hand, if the contact angle violates this condition in some area(s) of the contact line, the contact line rearranges its shape to satisfy (1) and thus a temporary drop sliding occurs. If the flow is not strong enough, a new equilibrium interfacial shape is reached which shows a non-axisymmetric contact-line shape. In strong enough flows, (1) may not be satisfied under any contact-line shape and the drop slips away.

The fundamental issues associated with the yield criteria for drop displacement from rigid boundaries (i.e. the equilibrium conditions just before the final drop dislodging) have been addressed in a series of papers by Dussan V. and coworkers (Dussan V. & Chow 1983; Dussan V. 1985, 1987), and Dimitrakopoulos & Higdon (1997, 1998, 1999, 2001, 2003). Dussan V.'s analysis for shear-flow displacement was based on asymptotic theory valid for very small contact angles and much smaller hysteresis (Dussan V. 1987). Dimitrakopoulos & Higdon (1997, 1998, 1999, 2001, 2003) considered stationary interfaces on solid surfaces and identified the yield criteria for displacement of fluid droplets and bridges. In their studies, the authors determined the optimal shape of the contact line which withstands the maximum external forcing, e.g. flow rate or gravitational force. Several physical systems were considered, including shear- and pressure-driven flows at low Reynolds number and the gravitational effects on fluid droplets attached to inclined solid surfaces. These studies considered a wide range of the parameters affecting these systems, i.e. viscosity ratio λ, capillary number Ca, Bond number B_d and advancing and receding contact angles. Comparison of the numerical results with asymptotic theories revealed that the useful range of the lubrication models is (quantitatively) extremely limited.

Several studies have considered the drop deformation under fixed constant line conditions for two- and three-dimensional interfaces. Feng & Basaran (1994) conducted a detailed study of the bubble displacement problem for steady two-dimensional flows at arbitrary Reynolds number. Schleizer & Bonnecaze (1999) studied the problem of deformation and sliding in viscous shear- and pressure-driven flows for two-dimensional droplets. Spelt (2006) considered pinned and moving two-dimensional droplets on an adhering channel at moderate-Reynolds-number shear flows. Owing to the restriction at two dimensions where the contact line degenerates into two contact points, the equilibrium conditions found in these studies may characterize the conditions both before the initial sliding and before the final drop dislodging. Li & Pozrikidis (1996) studied the shear-induced deformation of three-dimensional droplets with viscosity ratio $\lambda = 1$ adhering to solid substrates with fixed circular or elliptical contact lines. Yon & Pozrikidis (1999) extended the previous study by considering the influence of

the viscosity ratio λ and the effect of insoluble surfactants on the droplet deformation. These studies by Pozrikidis and coworkers considered the droplet deformation at the initial stage, i.e. before the onset of sliding. We emphasize that, although some information was presented for the transient deformation under subcritical and supercritical flow conditions (mainly the drop shape evolution), the earlier studies on two- and three-dimensional interfaces concentrated their interest on identifying the equilibrium interfacial properties as the capillary number increases. Thus, the conditions for the onset of interfacial sliding under contact angle hysteresis were not identified.

A wealth of studies have considered the dynamics of droplet sliding under flow or gravitational forcing. A review on drop sliding may be found in Dussan V. (1979), Shikhmurzaev (1997) and Spelt (2006). Several computational studies have considered the sliding dynamics of (mostly two-dimensional) droplets at both low- and finite-Reynolds-number flows (e.g. Schleizer & Bonnecaze 1999; Spelt 2006; Zhang, Miksis & Bankoff 2006). These studies commonly ignored the contact angle hysteresis; in this case, even the slightest external forcing is able to cause interfacial sliding. To the best of our knowledge, the conditions for the onset of sliding on rough surfaces have never been identified or used in these studies. This omission becomes more important if we consider that most experimental studies have concentrated on the problem of gravitational displacement.

Therefore, to understand the contact line motion on rough surfaces, we should first study the onset of interfacial sliding. To achieve this, in the present study we consider the deformation of a three-dimensional droplet attached to a rough surface as it deforms owing to a steady shear flow at low Reynolds number. The initial drop shape is a spherical cap forming a constant contact angle θ_0 (with $\theta_R \leqslant \theta_0 \leqslant \theta_A$) around a circular contact line. The main interest of the current study is to identify the portion(s) of the contact line where the hysteresis condition, (1), is first violated, i.e. the portion(s) of the contact line which will slide first. We also consider the transient evolution of the droplet shape as well as that of the contact angles around the initial circular contact line, and we identify the effects of the viscosity ratio.

We emphasize that for the problem studied in this paper, the onset of interfacial sliding cannot be inferred from the knowledge of the equilibrium contact angle distribution at gradually increasing flow rates. In particular, the interfacial sliding may occur during the transient evolution, depending on the flow rate, the physical parameters of the material system (i.e. θ_R, θ_A and the viscosity ratio) as well as the initial angle θ_0.

To address this problem, we employ our fully implicit time integration algorithm for interfacial dynamics in Stokes flow. Our method is based on a mathematically rigorous combination of implicit schemes with our Jacobian-free three-dimensional Newton method (Dimitrakopoulos & Higdon 1998), and thus it has strong stability properties which permit the use of large time steps.

After the mathematical formulation of multiphase flows in the Stokes regime, in § 2 we present a brief review of our implicit interfacial spectral boundary-element method. In § 3, we apply our numerical algorithm for the study of the dynamics of droplets attached to rough or chemically inhomogeneous solid substrates with a circular contact line as they are deformed in subcritical and supercritical simple shear flows. Our study reveals that droplets with small and moderate initial angles show an early period where both upstream and downstream sliding are equally favourable, as well as a late downstream-favored period. By contrast, droplets with large initial angles, after a rather small early equally favourable period, show a large period where downstream sliding is more favourable than the upstream sliding. In addition, droplets with intermediate initial angles are shown to be more stable owing to the

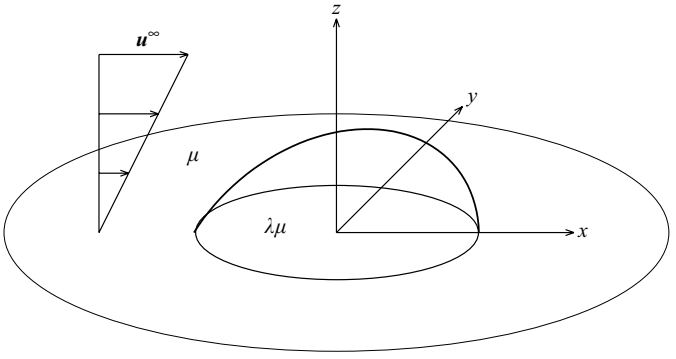

FIGURE 1. A fluid droplet attached to a solid boundary in a viscous shear flow.

surface tension force. The viscosity ratio is found to produce similar behaviour with respect to the onset of interfacial sliding; however, higher-viscosity droplets show a slower deformation rate, but a higher equilibrium interfacial deformation due to the increased viscous stress. An asymptotic behaviour for very small or large viscosity ratios is shown to exist.

2. Mathematical formulation and computational algorithm

2.1. *Mathematical formulation of viscous multiphase flows*

We consider a three-dimensional droplet attached to an infinite plane solid wall surrounded by a viscous fluid (figure 1). Initially, the fluids are at hydrostatic equilibrium while the drop shape is a spherical cap forming a constant contact angle $\theta = \theta_0$ (measured from within the drop phase) around a circular contact line. The droplet (fluid 1) has density ρ_1 and viscosity $\lambda\mu$, while the surrounding fluid (fluid 2) has density ρ_2 and viscosity μ. The droplet size is specified by its volume V or equivalently by the radius a of a spherical droplet of volume $4\pi a^3/3 = V$. The acceleration due to gravity is g while the surface tension γ is assumed constant. At time $t = 0$, a steady shear flow $\boldsymbol{u}^\infty = (Gz, 0, 0)$, where G is the shear rate, is introduced into the system causing interfacial deformation. In our study, the time is scaled with the flow time scale $\tau_f = G^{-1}$.

The capillary number Ca and Bond number B_d are defined by

$$Ca = \frac{\mu G a}{\gamma}, \qquad B_d = \frac{(\rho_1 - \rho_2) g a^2}{\gamma}. \tag{2}$$

These dimensionless parameters represent the ratio of viscous flow forces and gravitational forces to interfacial forces, respectively. Note that the length scale a used in the definition of the two dimensionless parameters above is based on the droplet volume V. The choice of this length scale is motivated by our interest in describing the physics of a specific fluid volume V which may be attached on a solid surface in many possible initial configurations (i.e. different angles θ_0) and undergo simple shear flow at different flow rates (or Ca).

The governing equations in fluid 2 are the Stokes equations together with continuity

$$\nabla \cdot \boldsymbol{\sigma} = -\nabla p + \mu \nabla^2 \boldsymbol{u} = 0, \tag{3}$$

$$\nabla \cdot \boldsymbol{u} = 0, \tag{4}$$

while in the droplet, the same equations apply with the viscosity replaced by $\lambda\mu$.

The boundary condition on the solid wall gives

$$\boldsymbol{u} = 0 \quad \text{on} \quad z = 0, \tag{5}$$

while far from the droplet

$$\boldsymbol{u} = \boldsymbol{u}^{\infty}. \tag{6}$$

At the interface, the boundary conditions on the velocity $\boldsymbol{u}$ and surface stress $\boldsymbol{f}$ are

$$\boldsymbol{u}_1 = \boldsymbol{u}_2, \tag{7}$$

$$\Delta \boldsymbol{f} = \boldsymbol{f}_2 - \boldsymbol{f}_1 = \gamma(\nabla \cdot \boldsymbol{n})\boldsymbol{n} + (\rho_2 - \rho_1)(\boldsymbol{g} \cdot \boldsymbol{x})\boldsymbol{n}. \tag{8}$$

Here the subscripts designate quantities evaluated in fluids 1 and 2, respectively. The surface stress is defined as $\boldsymbol{f} = \boldsymbol{\sigma} \cdot \boldsymbol{n}$ where $\boldsymbol{n}$ is the unit normal which we choose to point into fluid 2. The pressure as defined in $\boldsymbol{\sigma}$ is the dynamic pressure; hence the gravity force is absent from (3) and appears in the interfacial stress boundary condition, (8).

The time evolution of the interfacial shape may be determined via the kinematic condition at the interface

$$\frac{\mathrm{d}\boldsymbol{x}}{\mathrm{d}t} = (\boldsymbol{u} \cdot \boldsymbol{n})\,\boldsymbol{n}. \tag{9}$$

Although the governing equations and boundary conditions are linear in $\boldsymbol{u}$ and $\boldsymbol{f}$, the problem of determining the dynamic droplet shape constitutes a nonlinear problem, i.e. the velocity $\boldsymbol{u}$, stress $\boldsymbol{f}$ and curvature $\nabla \cdot \boldsymbol{n}$ are nonlinear functions of the geometrical variables describing the interface shape.

2.2. *Implicit interfacial spectral boundary-element method*

Since the pioneering work of Acrivos and coworkers (Youngren & Acrivos 1976; Rallison & Acrivos 1978), a common way to solve the interfacial problem presented in § 2.1, is by transforming the partial differential equations, (3) and (4), into boundary-integral equations, and using an explicit time-integration scheme for the determination of the interfacial evolution. The main benefit of this transformation is the great reduction in computational time since a fully three-dimensional problem can be described and solved using only two (curvilinear) coordinates.

In particular, the flow over the drop interface S_0 may be described by the integral formula

$$\begin{aligned}\Omega \boldsymbol{u}(\boldsymbol{x}_0) - \Omega_{\infty}\boldsymbol{u}^{\infty}(\boldsymbol{x}_0) = &- \int_{S_2} [\boldsymbol{S} \cdot (\boldsymbol{f}_2 - \boldsymbol{f}^{\infty}) - \mu \boldsymbol{T} \cdot (\boldsymbol{u}_2 - \boldsymbol{u}^{\infty}) \cdot \boldsymbol{n}]\,\mathrm{d}S \\ &+ \int_{S_1} [\boldsymbol{S} \cdot \boldsymbol{f}_1 - \lambda\mu \boldsymbol{T} \cdot \boldsymbol{u}_1 \cdot \boldsymbol{n}]\,\mathrm{d}S \\ &- \int_{S_0} [\boldsymbol{S} \cdot (\Delta \boldsymbol{f} - \boldsymbol{f}^{\infty}) - \mu \boldsymbol{T} \cdot ((1-\lambda)\boldsymbol{u} - \boldsymbol{u}^{\infty}) \cdot \boldsymbol{n}]\,\mathrm{d}S, \end{aligned} \tag{10}$$

where S_1 is the portion of the solid surface wetted by the drop and S_2 the remaining solid surface (Dimitrakopoulos & Higdon 1998). Note that $\boldsymbol{S}$ is the fundamental solution for the three-dimensional Stokes equations and $\boldsymbol{T}$ the associated stress. The coefficient Ω takes values $4\pi\mu(1+\lambda)$, $4\pi\lambda\mu$ and $4\pi\mu$ for points $\boldsymbol{x}_0$ on the surfaces S_0, S_1 and S_2, respectively, while Ω_{∞} takes the value $4\pi\mu$ for points $\boldsymbol{x}_0$ on the surfaces S_0 and S_2, and zero for points on the surface S_1.

In order to determine the droplet shape as a function of time, an explicit time-integration scheme may be employed to solve the kinematic condition at the interface,

(9). However, to ensure numerical stability, the employed time step must be smaller than any (numerical or physical) time scale appearing in the computational problem. The smallest time scale is commonly of a numerical nature, associated with the numerical discretization and in dimensionless form it may be written as

$$\Delta t < O(Ca\,\Delta x_{min}) \tag{11}$$

where Δx_{min} is the minimum grid spacing appearing in the computational problem, e.g. as discussed in Rallison (1981), Zinchenko & Davis (2005).

To avoid the associated penalty of the large number of time steps required to monitor the deformation of the fluid interface, we have developed an efficient fully implicit time-integration algorithm for interfacial dynamics in Stokes flow. Our method is based on a mathematically rigorous combination of implicit schemes with our Jacobian-free three-dimensional Newton method (Dimitrakopoulos & Higdon 1998). We employ both multi-step (one-stage) implicit formulae (e.g. Euler and backward differentiation schemes) and the multi-stage diagonally implicit Runge–Kutta schemes. (More details on these schemes may be found in Alexander 1997 and Butcher 2003).

By combining an implicit scheme with our Newton method, the resulting interfacial algorithm preserves the stability properties of the corresponding implicit formula, and thus it has strong stability properties which permit the use of very large time steps. In addition, we can easily achieve sufficient accuracy, even with large time steps, by employing high-order implicit schemes. See Dimitrakopoulos (2007) for more details on the implicit interfacial method.

The numerical solution of our implicit algorithm is achieved through an extension of the spectral boundary-element method described in Dimitrakopoulos & Higdon (1998) and Muldowney & Higdon (1995). The initial interface is divided into a moderate number N_E of elements. The geometric variables on each element are discretized using Lagrangian interpolation in terms of parametric variables ξ, η on the square interval $[-1, 1]^2$, e.g.

$$\boldsymbol{x}(\xi, \eta) = \sum_{i=1}^{N_B} \sum_{j=1}^{N_B} \boldsymbol{x}(\xi_i, \eta_j) h_i(\xi)\, h_j(\eta), \tag{12}$$

where h_i is the $(N_B - 1)$-order Lagrangian interpolant polynomial. The physical variables $\boldsymbol{u}$ and $\boldsymbol{f}$ are represented similarly. The base points (ξ_i, η_j) for the interpolation are chosen as the zeros of N_B-order orthogonal polynomials. This is equivalent to an orthogonal polynomial expansion and yields the spectral convergence associated with such expansions.

The boundary-integral equations, e.g. (10), admit two different types of points. The collocation points $\boldsymbol{x}_0$ of the left-hand side where the equation is required to hold and the basis points $\boldsymbol{x}$ of the right-hand side where the physical variables $\boldsymbol{u}$ and $\boldsymbol{f}$ are defined. The spectral-element method as implemented here employs collocation points of Gauss quadrature, i.e. in the interior of the element. As a result the boundary-integral equations hold even for singular elements, i.e. the elements which contain the contact line where the normal vector is not uniquely defined.

By combining the implicit interfacial method with the spectral boundary-element discretization, the resulting algorithm exploits all the benefits of the spectral methods, i.e. high-order interpolation with exponential convergence and numerical stability with increasing number of spectral points, along with the versatility of the boundary-element method, i.e. the ability to handle the most complicated geometries. In addition,

it is not affected by the disadvantage of the spectral methods used in volume discretization; namely, the requirement to deal with dense systems, because in boundary-integral formulations the resulting systems are always dense, independent of the form of the discretization. We note that the exponential convergence in the numerical accuracy is evident at both the properties of a given shape, such as the interfacial curvature, and the dynamic evolution of the interfacial shape (Dimitrakopoulos 2007).

3. Results

In the present study, we describe the adherent droplets by employing a discretization of $N_E = 24$ spectral elements, similar to that employed in Dimitrakopoulos & Higdon (1998). The surface of the drop is projected onto a cube whose faces are subdivided into a total of 11 elements (figure 2*c*). The wetted area S_1 on the solid surface is discretized into five elements while the outer solid surface S_2 is discretized into two rows of four elements each. (See figure 3 in our earlier study.) In our computations, the outer solid surface (which formally should extend to infinity) covers an area of at least 10 times the radius of the contact line which is sufficient to produce negligible error in all cases.

The results we present in this section for low and moderate viscosity ratio, $\lambda \leqslant 1$, were derived by employing $N_B = 7$–9 basis points and the third-order diagonally implicit Runge–Kutta scheme (DIRK3) with $\Delta t = 0.1$. For droplets with high viscosity ratio ($\lambda = 10, 100$), larger time steps were employed (see caption of figure 7). The accuracy of our results was verified by employing smaller time steps (usually $\Delta t = 0.05, 0.02$) and different basis points, (i.e. $N_B = 7$–9). The three-dimensional droplet shapes presented here were derived from the actual spectral grid by spectrally interpolating to $N_B = 20$. The parameters affecting this problem have been described in § 2.1; since in this paper we consider droplets with $B_d = 0$, the problem depends on the capillary number Ca, the viscosity ratio λ and the initial angle θ_0.

Figure 2(*a*) shows the time evolution of the interfacial profile for an adherent droplet with $\lambda = 1$ and $\theta_0 = 90^\circ$ in simple shear flow with $Ca = 0.15$. In the upstream portion of the interface, the contact angle is reduced monotonically with time whereas the opposite happens in the downstream portion where the interface extends in the flow direction. This is also shown in figure 2(*b*) where we plot the variation of the contact angle around the circular contact line at several times. For this physical system, $Ca = 0.15$ constitutes a subcritical capillary number, i.e. the drop interface reaches equilibrium after an initial transient period. The rather well-deformed interfacial shape at equilibrium is shown at figure 2(*c*).

Figure 2(*b*) shows that for circular contact lines, the contact angle increases monotonically with the azimuthal angle ϕ from the upstream towards the downstream area of the contact line at all times. (The azimuthal angle ϕ is measured with respect to the positive x-direction as usual.) The smallest contact angle θ_u occurs at $\phi = 180^\circ$ whereas the largest angle θ_d occurs at $\phi = 0^\circ$. Thus, to identify which portion of the contact line slides first, it is sufficient to monitor the time evolution of the two extreme angles, θ_u and θ_d.

Figure 3(*a*) shows the time evolution of the upstream and downstream contact angles, θ_u and θ_d as well as their difference $\theta_d - \theta_u$. This figure clearly reveals that $Ca = 0.15$ is a subcritical capillary number; after the initial transient evolution, both angles reach equilibrium where the interfacial shape does not change with time. Observe that this flow rate causes significant interfacial deformation (as shown in

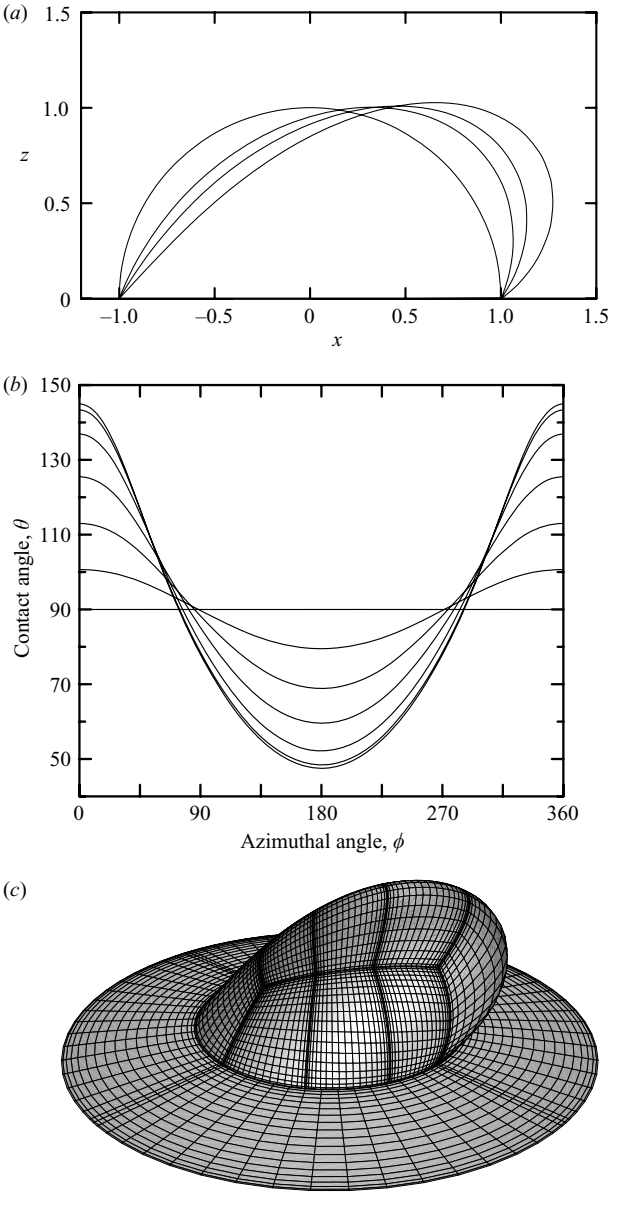

FIGURE 2. Deformation of an adherent droplet with $\lambda = 1$ and $\theta_0 = 90^\circ$ in simple shear flow with $Ca = 0.15$. (*a*) Droplet profile at times $t = 0, 0.5, 1, 10$. (*b*) The variation of the contact angle θ as a function of the azimuthal angle ϕ for times $t = 0, 0.2, 0.5, 1, 2, 4, 10$. (*c*) Droplet shape at $t = 10$, i.e. at equilibrium.

figure 2) and a large variation of the contact angles, θ_u and θ_d, whose difference reaches $\theta_d - \theta_u \approx 97.5^\circ$ at equilibrium.

To demonstrate clearly the variation of the upstream and downstream contact angles over time, in figure 3(*b*) we plot their time evolution with respect to their initial value $\theta_0 = 90^\circ$. Observe that initially both variations, $\theta_0 - \theta_u$ and $\theta_d - \theta_0$, grow equally with time. Later, the downstream angle increases faster than the upstream one.

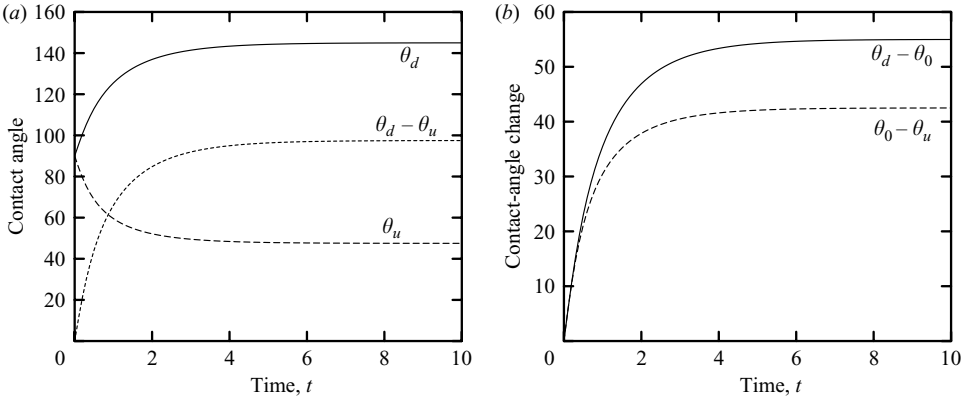

FIGURE 3. Deformation of an adherent droplet with $\lambda = 1$ and $\theta_0 = 90^\circ$ in simple shear flow with $Ca = 0.15$. (*a*) Time evolution of the upstream and downstream contact angles, θ_u and θ_d. Also included is the evolution of the difference $\theta_d - \theta_u$. (*b*) Time evolution of the upstream and downstream contact angle change, $\theta_0 - \theta_u$ and $\theta_d - \theta_0$.

Figure 3(*b*) constitutes probably the most important result with respect to the goals of this study. To explain the physical significance of this figure, we denote as θ_u^* and θ_d^* the value of the two angles at the end of the initial equal-growth period, while θ_u^{eq} and θ_d^{eq} denote the value of the angles at equilibrium, i.e. at the end of the unequal-growth period. Note that for this case, $\theta_0 - \theta_u^* \approx \theta_d^* - \theta_0 \approx 20^\circ$ while $\theta_0 - \theta_u^{eq} \approx 42.5^\circ$ and $\theta_d^{eq} - \theta_0 \approx 55^\circ$.

For real systems which exhibit the behaviour shown in figure 3(*b*), the advancing and receding angles, θ_A and θ_R, may fall into the following distinct regimes. The first case is when these angles fall in the equal-growth interval, i.e. $\theta_u^* \leqslant \theta_R < \theta_A \leqslant \theta_d^*$. In this case, if the droplet is placed on the solid forming an initial angle $\theta_0 < (\theta_R + \theta_A)/2$, then after some time the upstream portion of the drop will slide first. The opposite will happen if the initial angle is $\theta_0 > (\theta_R + \theta_A)/2$ where the downstream drop portion will begin moving on the solid substrate. In the limiting case of $\theta_0 = (\theta_R + \theta_A)/2$, both the downstream and the upstream portions may start sliding simultaneously. In general, we may conclude that for systems with $\theta_u^* \leqslant \theta_R < \theta_A \leqslant \theta_d^*$, both downstream and upstream sliding are equally favourable, and the first contact-line motion depends on the initial angle θ_0.

The second distinct regime is when the advancing and receding angles fall in the unequal-growth interval, i.e. $\theta_u^{eq} \leqslant \theta_R < \theta_u^* < \theta_d^* < \theta_A \leqslant \theta_d^{eq}$. In this case, the downstream sliding is more favourable than the upstream sliding, especially for advancing and receding angles close to the limits of the unequal-growth interval (i.e. $\theta_R \to \theta_u^{eq}$ and $\theta_A \to \theta_d^{eq}$). However, even in this case, the drop may begin to slide with its upstream portion if the initial angle θ_0 is close enough to θ_R.

In the last distinct regime, the advancing and receding angles fall outside the unequal-growth interval, i.e. $\theta_R < \theta_u^{eq} < \theta_d^{eq} < \theta_A$. In this case, the flow rate is not strong enough to initiate interfacial sliding and the droplet will remain attached to the solid surface with the original circular contact line.

In the case, when the advancing and receding angles fall into different regimes, the first contact-line motion may also be derived similarly. We emphasize that our conclusions above refer to systems which show an initial equal-growth period, followed by an unequal (downstream-favoured) growth period, as the one shown in figure 3(*b*). For a given viscosity ratio λ, the existence and size of these two growth regimes is

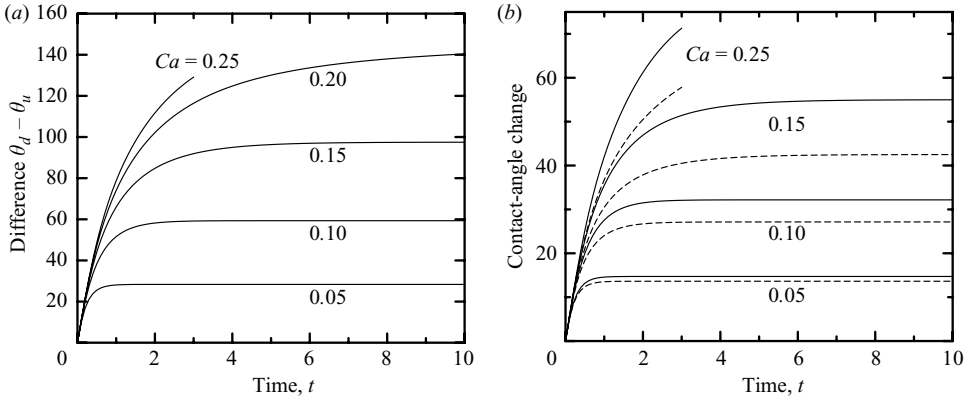

FIGURE 4. Influence of the capillary number Ca on the deformation of an adherent droplet with $\lambda = 1$ and $\theta_0 = 90°$ in simple shear flow. (a) Time evolution of the contact angle difference $\theta_d - \theta_u$ for $Ca = 0.05, 0.1, 0.15, 0.2, 0.25$. ($b$) Time evolution of the downstream and upstream contact angle change: ——, $\theta_d - \theta_0$; - - -, $\theta_0 - \theta_u$. The capillary number is $Ca = 0.05, 0.1, 0.15, 0.25$. (The behaviour for $Ca = 0.2$ is similar; the corresponding curves have been omitted for clarity.)

a function of the remaining system parameters, i.e. the capillary number Ca and the initial contact angle θ_0.

We investigate now the influence of the capillary number Ca on the deformation of adherent droplets. Figure 4(a) shows the time evolution of the contact-angle difference $\theta_d - \theta_u$ for a droplet with $\lambda = 1$ and $\theta_0 = 90°$, and for several capillary numbers. As the flow rate increases, the higher droplet deformation is accompanied with a monotonic increase in the contact-angle difference $\theta_d - \theta_u$ (up to equilibrium, if one exists). In addition, we observe that initially $\theta_d - \theta_u$ shows the same linear increase with time for any flow rate.

The explanation for the monotonic increase of the contact-angle difference $\theta_d - \theta_u$ with Ca becomes clear when the forces acting on the droplet are considered. Trying to balance the increased hydrodynamic force F_h is the component of interfacial force in the plane of the wall parallel to the flow direction. This force is proportional to the width (or radius) w of the contact region and, for small angle difference $\theta_d - \theta_u$, it scales as $F_\gamma \sim (\cos\theta_u - \cos\theta_d)\gamma w$. For small contact angles, this force takes the asymptotic form $(\theta_d - \theta_u)\theta_0 \gamma w$. Based on the volume of the drop, we have $V \sim a^3 \sim w^2 h$ where the height of the drop $h \sim w \tan\theta_0 \sim w\theta_0$ for small angles; thus, $w \sim a\theta_0^{-1/3}$. Therefore, for small contact angles and contact-angle difference $\theta_d - \theta_u$, the interfacial force scales as

$$F_\gamma \sim (\theta_d - \theta_u)\gamma a \theta_0^{2/3}. \tag{13}$$

To balance the hydrodynamic force F_h, the droplet must increase F_γ and thus the contact-angle difference $\theta_d - \theta_u$. For a droplet with an initial angle θ_0, as the capillary number Ca (and thus F_h) increases, the increased interfacial force is accompanied by a monotonic increase in the contact-angle difference $\theta_d - \theta_u$, in agreement with our numerical results (figure 4a).

Figure 4(b) shows the time evolution of the upstream and downstream contact-angle change, $\theta_0 - \theta_u$ and $\theta_d - \theta_0$, respectively. Several conclusions may be derived from this figure. First, both contact-angle changes show the same linear increase with time for any flow rate; thus initially, the dynamics upstream and downstream are the same, independently of the capillary number. We also conclude that adherent

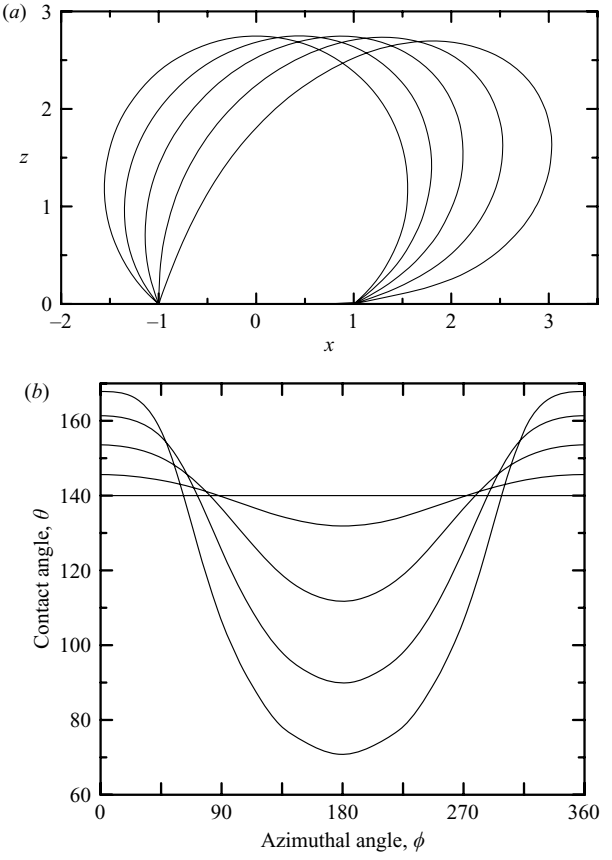

FIGURE 5. Deformation of an adherent droplet with $\lambda = 1$ and $\theta_0 = 140^\circ$ in simple shear flow with $Ca = 0.1$. (*a*) Droplet profile at times $t = 0, 0.2, 0.5, 1, 2$. (*b*) The variation of the contact angle θ as a function of the azimuthal angle ϕ for times $t = 0, 0.2, 0.5, 1, 2$.

droplets with $\theta_0 = 90^\circ$ show the two growth regimes (i.e. the equal growth and the downstream-favoured growth observed previously for $Ca = 0.15$) for both subcritical and supercritical Ca. In addition, figure 4(*b*) shows that as the flow rate increases, the relative size of the unequal growth regime (with respect to the size of the equal growth area) is increased. This is also evident in the larger variation of the downstream angle, $\theta_d - \theta_0$, compared to that of the upstream angle, $\theta_0 - \theta_u$, at equilibrium for subcritical capillary numbers as the flow rate increases.

We investigate now the influence of the initial angle θ_0 on the deformation of adherent droplets. Our computational results for droplets with $\theta_0 = 30^\circ, 50^\circ, 70^\circ, 100^\circ, 110^\circ$ reveal that the deformation of these droplets shows qualitatively similar behaviour to that for $\theta_0 = 90^\circ$ discussed previously (and thus the corresponding figures have been omitted.) On the other hand, droplets with large initial angles, i.e. $\theta_0 \geqslant 120^\circ$, show a different deformation behaviour. To show this, in figure 5 we present our results for a droplet with $\theta_0 = 140^\circ$ and $Ca = 0.1$. Observe that in this case, the downstream interfacial area tends to become tangential to the solid (figure 5*a*). A careful investigation of the variation of the contact angle around the contact line depicted in figure 5(*b*) reveals that the upstream interfacial area shows a greater contact-angle change than the downstream area.

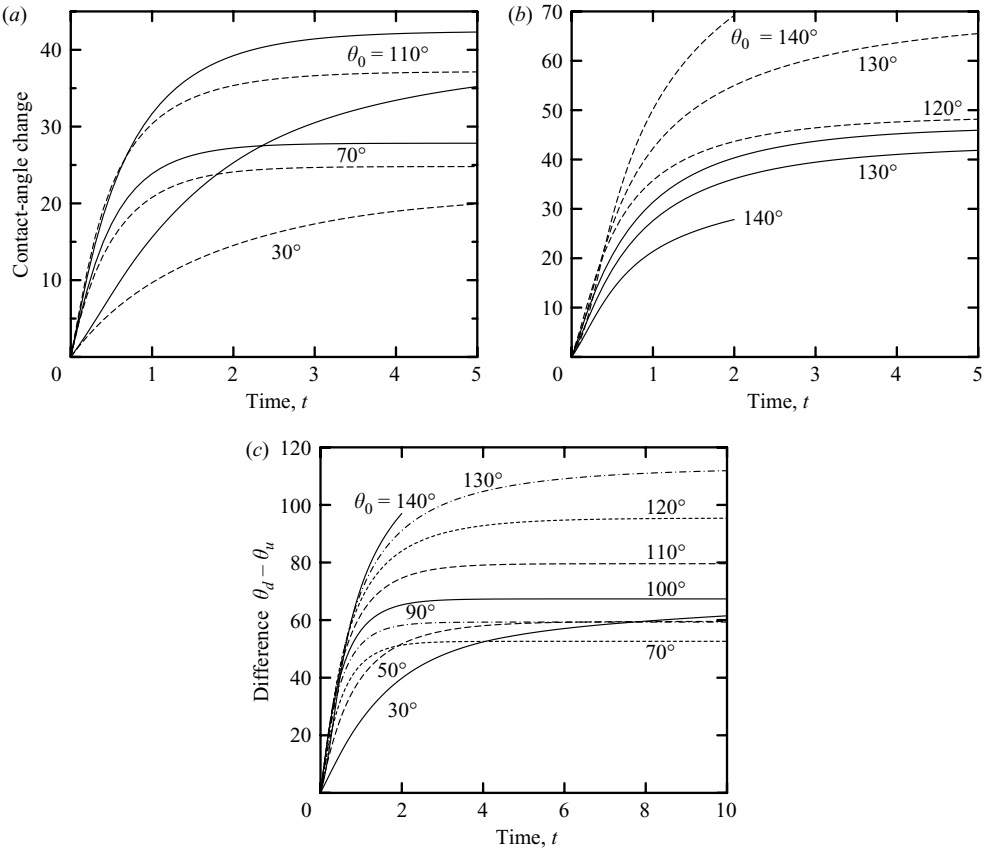

FIGURE 6. Influence of the initial angle θ_0 on the deformation of an adherent droplet with $\lambda = 1$ in simple shear flow with $Ca = 0.1$. (*a*) Time evolution of the downstream and upstream contact angle change: ——, $\theta_d - \theta_0$; - - -, $\theta_0 - \theta_u$. The initial angle is $\theta_0 = 30°, 70°, 110°$. (The behaviour for $\theta_0 = 50°, 90°, 100°$ is similar; the corresponding curves have been omitted for clarity.) (*b*) As in (*a*) but for $\theta_0 = 120°, 130°, 140°$. (*c*) Time evolution of the contact angle difference $\theta_d - \theta_u$ for $\theta_0 = 30°, \ldots, 140°$.

We collect now our results for the time evolution of the contact-angle downstream and upstream change, $\theta_d - \theta_0$ and $\theta_0 - \theta_u$, for different initial angles. Figure 6(*a*) shows this evolution for small and moderate initial angles $\theta_0 \leqslant 110°$ while in figure 6(*b*) we plot the time evolution of the contact-angle change for large angles $\theta_0 \geqslant 120°$. From this figure, it is evident that for small enough hysteresis, during the transient evolution, all drops with circular contact lines show an early period where both upstream and downstream sliding are equally favourable. During this regime, if the droplet is placed on the solid forming an initial angle $\theta_0 > (\theta_R + \theta_A)/2$, then after some time, the downstream portion of the drop will slide first. The opposite will happen if the initial angle is $\theta_0 < (\theta_R + \theta_A)/2$ where the upstream drop portion will begin moving on the solid substrate. Our numerical investigation shows that the initial equal-growth regime is more restricted for drops with large initial angles. For large enough hysteresis, drops with small and moderate initial angles θ_0 show a late downstream-favoured regime, where the downstream sliding occurs for initial angles $\theta_0 > \theta_0^*$ with $\theta_0^* < (\theta_R + \theta_A)/2$. By contrast, drops with large initial angles show a late

upstream-favoured regime, where the upstream sliding occurs for initial angles $\theta_0 < \theta_0^*$ with $\theta_0^* > (\theta_R + \theta_A)/2$.

An additional conclusion is also evident from the time evolution of the contact angle difference $\theta_d - \theta_u$, plotted in figure 6(*c*) for the different angles we have studied in the work. Initially, droplets with moderate and large angles show the same evolution whereas afterwards there is a monotonic increase in $\theta_d - \theta_u$ with θ_0 at the same time instance. On the other hand, later in time (e.g. near or at equilibrium) the droplet with $\theta_0 = 70^\circ$ shows the minimum contact-angle difference $\theta_d - \theta_u$, i.e. it is the most stable configuration.

Thus, droplets with intermediate initial angles are more stable than droplets with small or large initial angles. To explain this, consider that the interfacial force $F_\gamma \sim (\cos\theta_u - \cos\theta_d)\gamma w$ reaches its maximum value at $\theta_0 = 90^\circ$. Higher initial angles θ_0 reduce the net interfacial force leading to larger deformations and thus contact-angle difference $\theta_d - \theta_u$. This conclusion is in agreement with our numerical results shown in figure 6(*c*), which reveals that the minimum difference $\theta_d - \theta_u$ actually occurs at $\theta_0 = 70^\circ$. Thus, the fact that droplets with intermediate initial angles are more stable than droplets with small or large initial angles is associated with the interfacial force F_γ, as found for the optimal equilibrium shape of adherent drops (Dimitrakopoulos & Higdon 1998).

To investigate the effects of the viscosity of the fluids, we have studied droplets with different viscosity ratio (mainly $\lambda = 0, 1, 10$). With respect to the onset of interfacial sliding, the droplets with different viscosity ratio show similar behaviour and thus the corresponding figures for $\lambda \neq 1$ have been omitted. For a given flow rate Ca and initial angle θ_0, as the viscosity ratio increases from small values, the droplet shows a slower deformation rate (owing to the increased inner viscosity $\lambda\mu$), and a higher equilibrium interfacial deformation (if one exists) owing to the increased hydrodynamic force on the drop (i.e. the increased viscous stress). Both conclusions are evident in figure 7(*a*, *b*) where we plot the time evolution of the upstream and downstream contact angles, θ_u and θ_d, as well as the contact angle difference $\theta_d - \theta_u$, for a droplet with $\theta_0 = 90^\circ$ and $Ca = 0.12$, and for several viscosity ratios.

Observe that in figure 7(*a*, *b*) the time is scaled with $1+\lambda$. The reason for this scaling is that the dynamics of droplets with different viscosity ratio evolve on the surface tension time scale which may be described by $\tau_\gamma = (1+\lambda)\mu a/\gamma = (1+\lambda)Ca\tau_f$. Thus, the high-viscosity droplets show a much slower deformation rate than that for low-viscosity drops. Figure 7(*c*) shows the droplet profiles at equilibrium. As the viscosity ratio increases, the droplet shows a higher equilibrium interfacial deformation. For this initial angle θ_0, the downstream portion of the droplet tends to become tangential to the solid surface at high viscosity ratio (i.e. this flow rate is close to the critical value for high λ). We note that in figure 7 the curves for $\lambda = 0, 0.001$ are nearly coincident; the same is true for the high-viscosity curves $\lambda = 100, 1000$. This indicates that the droplet deformation shows asymptotic behaviour for very small or very large viscosity ratios.

As a closure, we note that the fact that the downstream sliding is more favourable for droplets with small and moderate initial angles during their late evolution period was identified in the earlier work of Li & Pozrikidis (1996) based on the equilibrium distribution of the contact angle around the contact line for several subcritical capillary numbers of droplets with $\theta_0 = 90^\circ$ (see their §4.1.2). However, as we discuss in the present study, the initiation of interfacial sliding is a more complicated phenomenon where under certain conditions both downstream and upstream sliding may be equally favourable or upstream sliding may be more favourable than downstream motion.

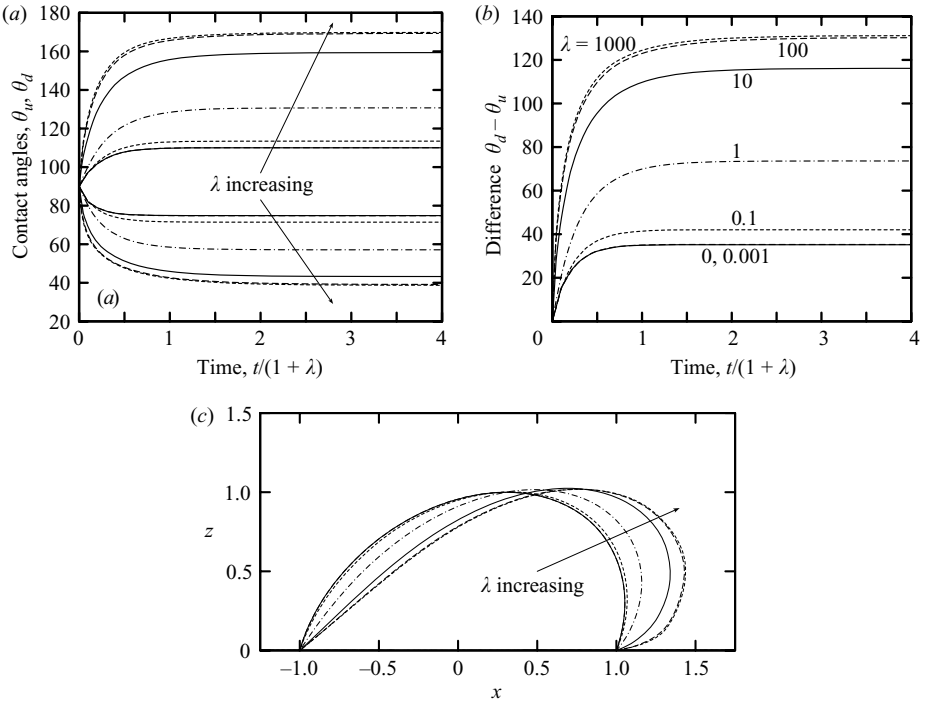

FIGURE 7. Influence of the viscosity ratio λ on the deformation of an adherent droplet with $\theta_0 = 90°$ in simple shear flow with $Ca = 0.12$. Viscosity ratio studied: $\lambda = 0, 0.001, 0.1, 1, 10, 100, 1000$. (*a*) Time evolution of the upstream and downstream contact angles, θ_u and θ_d. (*b*) Time evolution of the contact angle difference $\theta_d - \theta_u$. (*c*) Droplet profile at equilibrium. Note that the curves for $\lambda = 0, 0.001$ nearly coincide; the same happens for the curves for $\lambda = 100, 1000$. The results for $\lambda = 0, 0.001, 0.1, 1$ were obtained by employing $\Delta t = 0.1$ in the time interval [0, 20]. The results for $\lambda = 10, 100, 1000$ were obtained by employing $\Delta t = 0.5, 2, 20$ in the time interval [0, 50], [0, 400], [0, 4000], respectively.

4. Conclusions

In this paper, we have considered the dynamics of droplets attached to rough or chemically inhomogeneous solid substrates with a circular contact line as they are deformed in subcritical and supercritical simple shear flows. Our main interest was concentrated on identifying the portion(s) of the contact line where the contact-angle hysteresis condition is first violated, i.e. the portion(s) of the contact line which slide(s) first. To address this physical problem, we have employed our fully implicit time-integration algorithm for interfacial dynamics in Stokes flow. Our method is based on a mathematically rigorous combination of implicit schemes with our three-dimensional Newton method (Dimitrakopoulos & Higdon 1998), and thus it has strong stability properties which permit the use of large time steps.

Our study reveals that droplets with small and moderate initial angles show an early period where both upstream and downstream sliding are equally favourable, as well as a late downstream-favored period. By contrast, droplets with large initial angles, after a rather small early equally-favourable period, show a large period where downstream sliding is more favourable than upstream sliding. In addition, we show that due to the surface tension force, droplets with intermediate initial angles are more stable than droplets with small or large initial angles. Droplets with different viscosity ratio show similar behaviour with respect to the onset of interfacial sliding. As the viscosity

ratio increases from small values, the droplet shows a slower deformation rate but a higher equilibrium interfacial deformation (if one exists) owing to the increased hydrodynamic force. An asymptotic behaviour for very small or large viscosity ratios is shown to exist.

Our study provides insight into interfacial sliding for several multiphase flow systems including coating operations, enhanced oil recovery, microfluidics and biological systems. The problem of contact-line motion is truly three-dimensional since the contact line can expand or contract in the lateral (i.e. crossflow) direction changing the interfacial dynamics, as shown in Dimitrakopoulos & Higdon (1998, 1999, 2001), and the experiments of Podgorski, Flesselles & Limat (2001).

This work was supported in part by the National Science Foundation. Acknowledgment is made to the Donors of the American Chemical Society Petroleum Research Fund for partial support. Some computations were performed on multiprocessor supercomputers provided by the National Center for Supercomputing Applications (NCSA) in Illinois.

REFERENCES

Alexander, R. 1997 Diagonally implicit Runge–Kutta methods for stiff O.D.E.'s. *SIAM J. Numer. Anal.* **14**, 1006–1021.

Bear, J. 1972 *Dynamics of Fluids in Porous Media.* Dover.

Butcher, J. C. 2003 *Numerical Methods for Ordinary Differential Equations.* Wiley.

Cristini, V. & Tan, Y.-C. 2004 Theory and numerical simulation of droplet dynamics in complex flows – a review. *Lab Chip* **4**, 257–264.

Dimitrakopoulos, P. 2007 Interfacial dynamics in Stokes flow via a three-dimensional fully-implicit interfacial spectral boundary element algorithm. *J. Comput. Phys.* (in press).

Dimitrakopoulos, P. & Higdon, J. J. L. 1997 Displacement of fluid droplets from solid surfaces in low-Reynolds-number shear flows. *J. Fluid Mech.* **336**, 351–378.

Dimitrakopoulos, P. & Higdon, J. J. L. 1998 On the displacement of three-dimensional fluid droplets from solid surfaces in low-Reynolds-number shear flows. *J. Fluid Mech.* **377**, 189–222.

Dimitrakopoulos, P. & Higdon, J. J. L. 1999 On the gravitational displacement of three-dimensional fluid droplets from inclined solid surfaces. *J. Fluid Mech.* **395**, 181–209.

Dimitrakopoulos, P. & Higdon, J. J. L. 2001 On the displacement of three-dimensional fluid droplets adhering to a plane wall in viscous pressure-driven flows. *J. Fluid Mech.* **435**, 327–350.

Dimitrakopoulos, P. & Higdon, J. J. L. 2003 On the displacement of three-dimensional fluid bridges from solid surfaces in viscous pressure-driven flows. *Phys. Fluids* **15** (10), 3255–3258.

Dussan V., E. B. 1979 On the spreading of liquids on solid surfaces: static and dynamic contact lines. *Annu. Rev. Fluid Mech.* **11**, 371–400.

Dussan V., E. B. 1985 On the ability of drops or bubbles to stick to non-horizontal surfaces of solids. Part 2. Small drops or bubbles having contact angles of arbitrary size. *J. Fluid Mech.* **151**, 1–20.

Dussan V., E. B. 1987 On the ability of drops to stick to surfaces of solids. Part 3. The influences of the motion of the surrounding fluid on dislodging drops. *J. Fluid Mech.* **174**, 381–397.

Dussan V., E. B. & Chow, R. T.-P. 1983 On the ability of drops or bubbles to stick to non-horizontal surfaces of solids. *J. Fluid Mech.* **137**, 1–29.

Feng, J. Q. & Basaran, O. A. 1994 Shear flow over a translationally symmetric cylindrical bubble pinned on a slot in a plane wall. *J. Fluid Mech.* **275**, 351–378.

Greenspan, H. P. 1978 On the motion of a small viscous droplet that wets a surface. *J. Fluid Mech.* **84**, 125–143.

Hodges, S. R. & Jensen, O. E. 2002 Spreading and peeling dynamics in a model of cell adhesion. *J. Fluid Mech.* **460**, 381–409.

Hynes, R. O. 1992 Integrins, versatility, modulation and signaling in cell adhesion. *Cell* **69**, 11–25.

Li, X. & Pozrikidis, C. 1996 Shear flow over a liquid drop adhering to a solid surface. *J. Fluid Mech.* **307**, 167–190.

Muldowney, G. P. & Higdon, J. J. L. 1995 A spectral boundary element approach to three-dimensional Stokes flow. *J. Fluid Mech.* **298**, 167–192.

Podgorski, T., Flesselles, J.-M. & Limat, L. 2001 Corners, cusps, and pearls in running drops. *Phys. Rev. Lett.* **87**, 036102.

Rallison, J. M. 1981 A numerical study of the deformation and burst of a viscous drop in general shear flows. *J. Fluid Mech.* **109**, 465–482.

Rallison, J. M. & Acrivos, A. 1978 A numerical study of the deformation and burst of a viscous drop in an extensional flow. *J. Fluid Mech.* **89**, 191–200.

Schleizer, A. D. & Bonnecaze, R. T. 1999 Displacement of a two-dimensional immiscible droplet adhering to a wall in shear- and pressure-driven flows. *J. Fluid Mech.* **383**, 29–54.

Shikhmurzaev, Y. D. 1997 The moving contact line on a smooth solid surface. *J. Fluid Mech.* **334**, 211–249.

Spelt, P. D. M. 2006 Shear flow past two-dimensional droplets pinned or moving on an adhering channel wall at moderate Reynolds numbers: a numerical study. *J. Fluid Mech.* **561**, 439–463.

Stone, H. A., Stroock, A. D. & Ajdari, A. 2004 Engineering flows in small devices: microfluidics toward a lab-on-a-chip. *Annu. Rev. Fluid Mech.* **36**, 381–411.

Tan, Y.-C., Fisher, J. S., Lee, A. I., Cristini, V. & Lee, A. P. 2004 Design of microfluidic channel geometries for the control of droplet volume, chemical concentration, and sorting. *Lab Chip* **4**, 292–298.

Yon, S. & Pozrikidis, C. 1999 Deformation of a liquid drop adhering to a plane wall: significance of the drop viscosity and the effect of an insoluble surfactant. *Phys. Fluids* **11**, 1297–1308.

Youngren, G. K. & Acrivos, A. 1976 On the shape of a gas bubble in a viscous extensional flow. *J. Fluid Mech.* **76**, 433–442.

Zhang, J., Miksis, M. J. & Bankoff, S. G. 2006 Nonlinear dynamics of a two-dimensional viscous drop under shear flow. *Phys. Fluids* **18**, 072106.

Zinchenko, A. Z. & Davis, R. H. 2005 A multipole-accelerated algorithm for close interaction of slightly deformable drops. *J. Comput. Phys.* **207**, 695–735.